**Send requests/inquiries to sjkeihm@gmail.com**

# MICROWAVE BRIGHTNESS TEMPERATURES OF THE MOON: THE APOLLO MODEL

Stephen J. Keihm

This web page provides examples of model-generated lunar brightness temperatures (TBs) as viewed from the Earth, including disk center, disk average, and digital mapping results. **The intent of the web page is to alert the radio telescope and planetary science community of a free available resource for using the moon as a calibration reference as well as a tool for mapping variations of the lunar thermal and electrical properties of the upper ~ 1 meter of regolith.** The model generated brightness temperatures have been used as calibration references since the 1980s by a large number of radio science projects and missions, including NASA's Deep Space Network (1-5), the Cosmic Background Explorer mission (6,7), the Microwave Limb Sounder of NASA's Earth Observing System (8), and the millimeter wave radiometers on the European Space Agency's Odin and Steam-R satellites (9,10).

The lunar regolith property model used to generate the predicted brightness temperatures is based on analyses of the Apollo 15 and 17 Heat Flow Experiment data (11-15) as well as thermophysical and electrical property measurements of returned Apollo samples (16-26). Validation of the model was provided by extensive comparisons with Earth-based microwave measurements of the lunar frontside (27-30). A recent confirmation of the model was provided by the Diviner Lunar Radiometer Experiment (31). Details of the lunar regolith model, including depth and temperature dependencies of the relevant thermal and electrical properties, can be found in the appendix of reference 32. Analyses of second order scattering effects, neglected in the current model, can be found in references 33 and 34.

The regolith model is considered regionally uniform over the lunar front side. Bond albedo contrasts of a factor of ~ 2 are known to exist between mare and highland regions, producing daytime surface temperature differences of ~ +/-4 K relative to the uniform model. The albedo-induced contrasts are lessened at the microwave wavelengths. Mare-highland contrasts in electrical absorption properties have also been inferred (ref [x]), producing brightness temperature anomalies of ~ +/- 3-4 K at X-band in regions of the full moon. These regional variations lie well within the estimated absolute accuracy (+/- 5%) of the Apollo-based model predictions.

Sample outputs of the Apollo-based lunar regolith model, presented as brightness temperatures (TBs), are shown below. All TB values represent Planck black body brightness temperatures; i.e. the calculations weighted Planck fluxes over all relevant regolith depths and the spectral radiation can be computed from the Planck function for specified wavelength and TB values. Libration and annual effects, less than ~ 3 K deviations in the TBs, are neglected. Figure 1 shows the model-predicted TB phase variations at the lunar frontside center over the 1 mm to 10 cm range. Figure 2 shows the disk-averaged TB phase variations over the same wavelength range. Figures 3 and 4 display digital maps of the model predicted pencil beam TBs at

1.8 mm wavelength at the full moon (Fig. 3) and new moon (Fig. 4) phases.

**Similar data sets and digital maps can be easily generated at specified wavelengths and lunar phases upon request. Send requests/inquiries to sjkeihm@gmail.com**

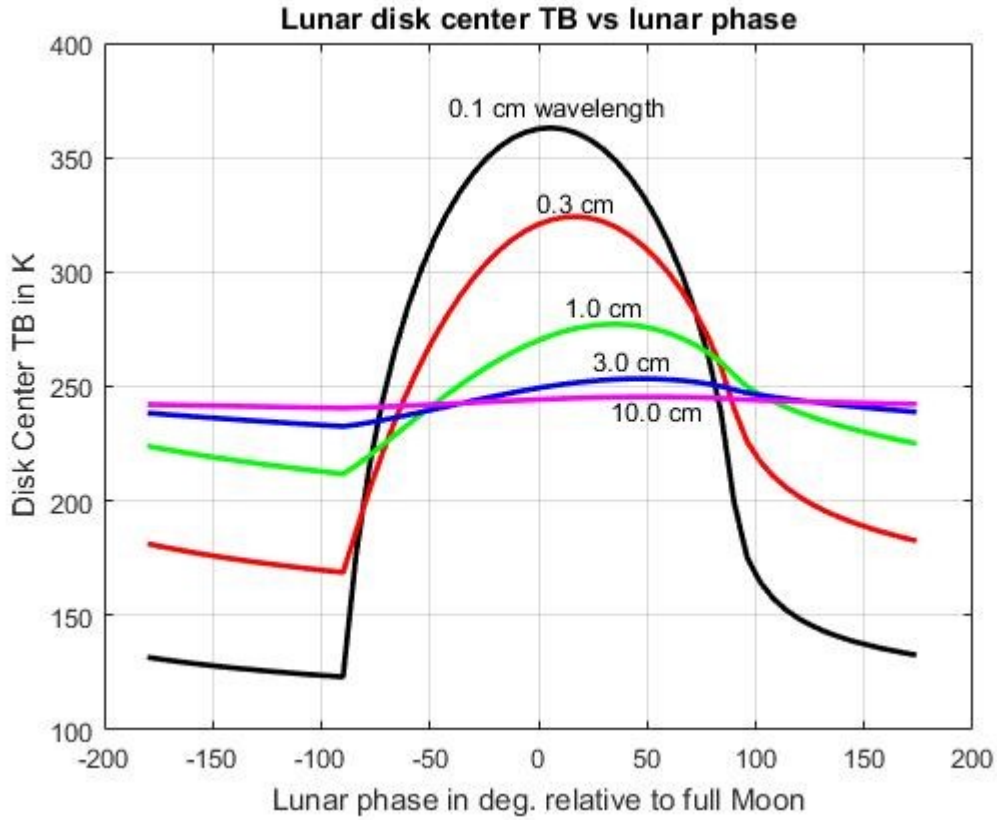


**Figure 1.** Model-generated pencil beam brightness temperatures of the lunar frontside disk center vs. lunar phase for wavelengths from 1 mm to 10 cm

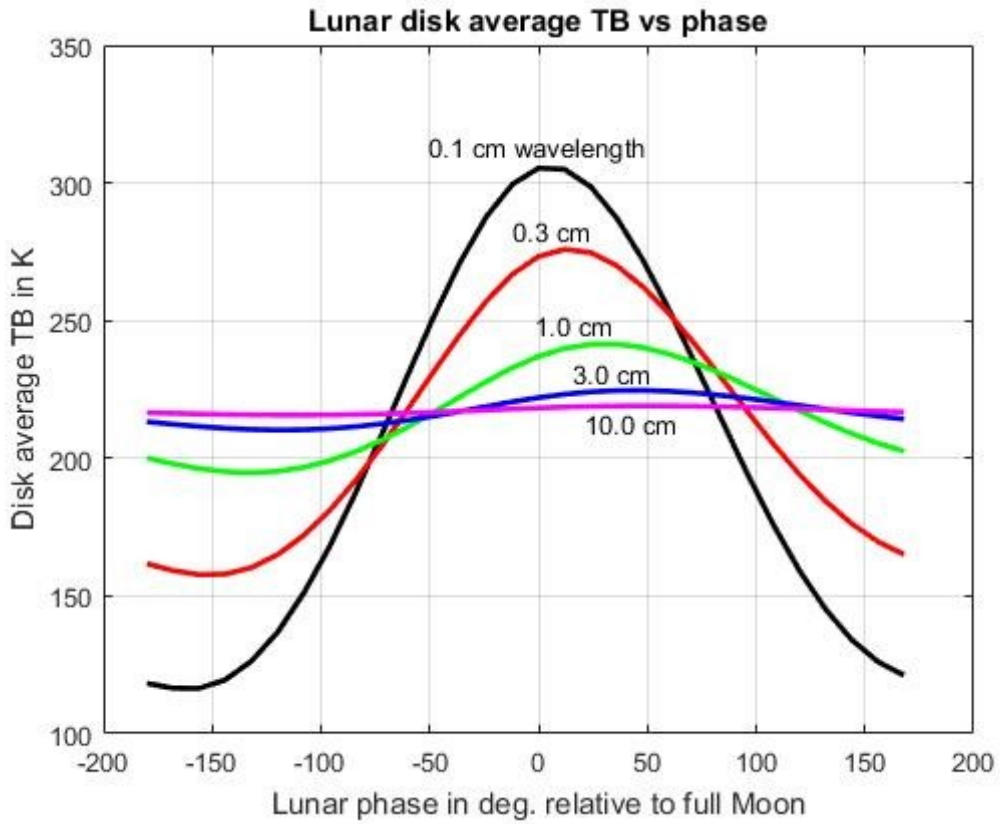


**Figure 2.** Model-generated disk average brightness temperatures of the lunar frontside vs. lunar phase for wavelengths from 1 mm to 10 cm

| | | | | | | | | | | | | | | | | | | |
|---|---|---|---|---|---|---|---|---|---|---|---|---|---|---|---|---|---|---|
| 0.00 | 0.00 | 0.00 | 0.00 | 0.00 | 134.49 | 198.88 | 227.60 | 241.90 | 248.11 | 247.57 | 239.18 | 216.82 | 157.82 | 0.00 | 0.00 | 0.00 | 0.00 | 0.00 |
| 0.00 | 0.00 | 0.00 | 78.08 | 203.50 | 244.20 | 264.92 | 277.09 | 284.46 | 288.45 | 289.17 | 286.65 | 279.65 | 264.67 | 230.57 | 103.47 | 0.00 | 0.00 | 0.00 |
| 0.00 | 0.00 | 104.32 | 223.46 | 260.12 | 279.75 | 292.01 | 300.04 | 305.29 | 308.48 | 309.52 | 308.56 | 305.05 | 297.69 | 283.62 | 253.52 | 135.71 | 0.00 | 0.00 |
| 0.00 | 54.06 | 223.10 | 264.13 | 285.21 | 298.57 | 307.39 | 313.61 | 317.93 | 320.69 | 321.86 | 321.51 | 319.41 | 314.98 | 306.51 | 291.05 | 256.83 | 76.82 | 0.00 |
| 0.00 | 202.37 | 258.87 | 284.32 | 299.76 | 309.95 | 317.24 | 322.55 | 326.31 | 328.80 | 330.03 | 330.03 | 328.61 | 325.41 | 319.65 | 309.28 | 289.81 | 240.45 | 0.00 |
| 124.81 | 241.49 | 277.09 | 296.50 | 308.86 | 317.58 | 323.96 | 328.68 | 332.08 | 334.39 | 335.65 | 335.86 | 334.85 | 332.38 | 327.85 | 320.13 | 306.21 | 277.31 | 163.11 |
| 196.04 | 260.46 | 288.04 | 304.07 | 314.92 | 322.74 | 328.54 | 332.88 | 336.03 | 338.22 | 339.50 | 339.85 | 339.11 | 337.08 | 333.29 | 326.86 | 315.91 | 294.60 | 237.33 |
| 222.44 | 271.13 | 294.42 | 308.86 | 318.83 | 326.10 | 331.49 | 335.58 | 338.59 | 340.73 | 341.99 | 342.41 | 341.84 | 340.13 | 336.79 | 331.10 | 321.56 | 304.11 | 262.69 |
| 234.24 | 276.61 | 297.93 | 311.52 | 321.02 | 327.92 | 333.13 | 337.09 | 340.04 | 342.14 | 343.40 | 343.85 | 343.36 | 341.78 | 338.74 | 333.45 | 324.64 | 308.97 | 273.76 |
| 237.67 | 278.27 | 299.05 | 312.39 | 321.73 | 328.51 | 333.65 | 337.58 | 340.52 | 342.59 | 343.86 | 344.32 | 343.85 | 342.32 | 339.38 | 334.21 | 325.61 | 310.44 | 276.95 |
| 234.24 | 276.61 | 297.93 | 311.52 | 321.02 | 327.92 | 333.13 | 337.09 | 340.04 | 342.14 | 343.40 | 343.85 | 343.36 | 341.78 | 338.74 | 333.45 | 324.64 | 308.97 | 273.76 |
| 222.44 | 271.13 | 294.42 | 308.86 | 318.83 | 326.10 | 331.49 | 335.58 | 338.59 | 340.73 | 341.99 | 342.41 | 341.84 | 340.13 | 336.79 | 331.10 | 321.56 | 304.11 | 262.69 |
| 196.04 | 260.46 | 288.04 | 304.07 | 314.92 | 322.74 | 328.54 | 332.88 | 336.03 | 338.22 | 339.50 | 339.85 | 339.11 | 337.08 | 333.29 | 326.86 | 315.91 | 294.60 | 237.33 |
| 124.81 | 241.49 | 277.09 | 296.50 | 308.86 | 317.58 | 323.96 | 328.68 | 332.08 | 334.39 | 335.65 | 335.86 | 334.85 | 332.38 | 327.85 | 320.13 | 306.21 | 277.31 | 163.11 |
| 0.00 | 202.37 | 258.87 | 284.32 | 299.76 | 309.95 | 317.24 | 322.55 | 326.31 | 328.80 | 330.03 | 330.03 | 328.61 | 325.41 | 319.65 | 309.28 | 289.81 | 240.45 | 0.00 |
| 0.00 | 54.06 | 223.10 | 264.13 | 285.21 | 298.57 | 307.39 | 313.61 | 317.93 | 320.69 | 321.86 | 321.51 | 319.41 | 314.98 | 306.51 | 291.05 | 256.83 | 76.82 | 0.00 |
| 0.00 | 0.00 | 104.32 | 223.46 | 260.12 | 279.75 | 292.01 | 300.04 | 305.29 | 308.48 | 309.52 | 308.56 | 305.05 | 297.69 | 283.62 | 253.52 | 135.71 | 0.00 | 0.00 |
| 0.00 | 0.00 | 0.00 | 78.08 | 203.50 | 244.20 | 264.92 | 277.09 | 284.46 | 288.45 | 289.17 | 286.65 | 279.65 | 264.67 | 230.57 | 103.47 | 0.00 | 0.00 | 0.00 |
| 0.00 | 0.00 | 0.00 | 0.00 | 0.00 | 134.49 | 198.88 | 227.60 | 241.90 | 248.11 | 247.57 | 239.18 | 216.82 | 157.82 | 0.00 | 0.00 | 0.00 | 0.00 | 0.00 |

**Figure 3.** Model-generated digital brightness temperature map of the full moon at a wavelength of 1.8 mm. The digital pencil beam TB values are separated by 0.1 lunar disk radii in the lunar frontside image plane. Note the north-south (top to bottom) symmetry (libration effects neglected) and east-west (right to left) asymmetry due to the diurnal phase lag.

| | | | | | | | | | | | | | | | | | | |
|---|---|---|---|---|---|---|---|---|---|---|---|---|---|---|---|---|---|---|
| 0.00 | 0.00 | 0.00 | 0.00 | 0.00 | 91.79 | 108.87 | 113.04 | 113.75 | 112.85 | 110.63 | 106.57 | 98.46 | 77.00 | 0.00 | 0.00 | 0.00 | 0.00 | 0.00 |
| 0.00 | 0.00 | 0.00 | 75.11 | 124.15 | 130.62 | 132.14 | 132.16 | 131.49 | 130.35 | 128.77 | 126.59 | 123.43 | 118.23 | 107.00 | 56.19 | 0.00 | 0.00 | 0.00 |
| 0.00 | 0.00 | 95.12 | 136.82 | 141.60 | 142.54 | 142.38 | 141.75 | 140.84 | 139.69 | 138.33 | 136.65 | 134.50 | 131.54 | 126.86 | 117.27 | 71.97 | 0.00 | 0.00 |
| 0.00 | 63.10 | 142.80 | 148.38 | 149.41 | 149.24 | 148.66 | 147.85 | 146.89 | 145.77 | 144.51 | 143.06 | 141.29 | 139.05 | 135.99 | 131.02 | 120.23 | 44.28 | 0.00 |
| 0.00 | 142.46 | 152.52 | 154.23 | 154.22 | 153.71 | 152.98 | 152.11 | 151.13 | 150.06 | 148.86 | 147.51 | 145.95 | 144.05 | 141.60 | 138.11 | 132.07 | 116.01 | 0.00 |
| 115.11 | 153.68 | 157.42 | 157.86 | 157.51 | 156.85 | 156.05 | 155.16 | 154.20 | 153.14 | 152.00 | 150.71 | 149.25 | 147.53 | 145.40 | 142.56 | 138.18 | 129.27 | 86.29 |
| 145.87 | 158.58 | 160.30 | 160.30 | 159.77 | 159.04 | 158.23 | 157.33 | 156.38 | 155.36 | 154.24 | 153.00 | 151.59 | 149.98 | 148.02 | 145.51 | 141.89 | 135.45 | 116.48 |
| 154.02 | 161.13 | 162.12 | 161.87 | 161.26 | 160.49 | 159.68 | 158.80 | 157.86 | 156.84 | 155.73 | 154.53 | 153.17 | 151.60 | 149.75 | 147.42 | 144.18 | 138.83 | 125.76 |
| 157.30 | 162.45 | 163.11 | 162.75 | 162.10 | 161.35 | 160.53 | 159.65 | 158.71 | 157.70 | 156.60 | 155.40 | 154.06 | 152.53 | 150.73 | 148.49 | 145.46 | 140.59 | 129.71 |
| 158.24 | 162.87 | 163.42 | 163.04 | 162.38 | 161.63 | 160.80 | 159.93 | 158.99 | 157.97 | 156.88 | 155.69 | 154.36 | 152.84 | 151.05 | 148.84 | 145.86 | 141.15 | 130.85 |
| 157.30 | 162.45 | 163.11 | 162.75 | 162.10 | 161.35 | 160.53 | 159.65 | 158.71 | 157.70 | 156.60 | 155.40 | 154.06 | 152.53 | 150.73 | 148.49 | 145.46 | 140.59 | 129.71 |
| 154.02 | 161.13 | 162.12 | 161.87 | 161.26 | 160.49 | 159.68 | 158.80 | 157.86 | 156.84 | 155.73 | 154.53 | 153.17 | 151.60 | 149.75 | 147.42 | 144.18 | 138.83 | 125.76 |
| 145.87 | 158.58 | 160.30 | 160.30 | 159.77 | 159.04 | 158.23 | 157.33 | 156.38 | 155.36 | 154.24 | 153.00 | 151.59 | 149.98 | 148.02 | 145.51 | 141.89 | 135.45 | 116.48 |
| 115.11 | 153.68 | 157.42 | 157.86 | 157.51 | 156.85 | 156.05 | 155.16 | 154.20 | 153.14 | 152.00 | 150.71 | 149.25 | 147.53 | 145.40 | 142.56 | 138.18 | 129.27 | 86.29 |
| 0.00 | 142.46 | 152.52 | 154.23 | 154.22 | 153.71 | 152.98 | 152.11 | 151.13 | 150.06 | 148.86 | 147.51 | 145.95 | 144.05 | 141.60 | 138.11 | 132.07 | 116.01 | 0.00 |
| 0.00 | 63.10 | 142.80 | 148.38 | 149.41 | 149.24 | 148.66 | 147.85 | 146.89 | 145.77 | 144.51 | 143.06 | 141.29 | 139.05 | 135.99 | 131.02 | 120.23 | 44.28 | 0.00 |
| 0.00 | 0.00 | 95.12 | 136.82 | 141.60 | 142.54 | 142.38 | 141.75 | 140.84 | 139.69 | 138.33 | 136.65 | 134.50 | 131.54 | 126.86 | 117.27 | 71.97 | 0.00 | 0.00 |
| 0.00 | 0.00 | 0.00 | 75.11 | 124.15 | 130.62 | 132.14 | 132.16 | 131.49 | 130.35 | 128.77 | 126.59 | 123.43 | 118.23 | 107.00 | 56.19 | 0.00 | 0.00 | 0.00 |
| 0.00 | 0.00 | 0.00 | 0.00 | 0.00 | 91.79 | 108.87 | 113.04 | 113.75 | 112.85 | 110.63 | 106.57 | 98.46 | 77.00 | 0.00 | 0.00 | 0.00 | 0.00 | 0.00 |

**Figure 4.** Model-generated digital brightness temperature map of the new moon at a wavelength of 1.8 mm. The digital pencil beam TB values are separated by 0.1 lunar disk radii in the lunar frontside image plane. Note the north-south (top to bottom) symmetry (libration effects neglected) and east-west (right to left) asymmetry due to the diurnal phase lag.

## References:

1. Morabito, D.D. (1999), The Characterization of a 34-Meter Beam-Waveguide Antenna at Ka-band (32 GHz) and X-band (8.4 GHz), IEEE Antennas and Propagation Magazine, vol. 41, no. 4, pp. 23–34.

2. Morabito, D. D., "Lunar Noise-Temperature Increase Measurements at S-Band, X-Band, and Ka-Band Using a 34-Meter-Diameter Beam-Waveguide Antenna,"

IPN PR 42-166, pp. 1-18, Jet Propulsion Laboratory, August 15, 2006.

3. Imbriale, W. A., "Computing the Noise Temperature Increase Caused by Pointing DSS 13 at the Center of the Moon," IPN PR 42-166, pp. 1-10, Jet Propulsion Laboratory, August 15, 2006.

4. Morabito, D., M. Gatti, and H. Miyatake, "The Moon as a Calibration Load for the Breadboard Array," IPN PR 42-172, pp. 1-21, Jet Propulsion Laboratory, February 15, 2008.

5. Morabito, D. D., "Dynamic Telemetry Link Advantage When Tracking a Lunar Orbiter with a 34-m Antenna at 2.3 GHz and 8.4 GHz," IPN PR 42-200, pp. 1-17, Jet Propulsion Laboratory, February 15, 2015.

6. Collaboration with COBE Co-I Michael Janssen of the Jet Propulsion Laboratory, California Institute of Technology, Pasadena CA.

7. Jackson, P. et al. (1991), "COBE DMR Data processing Techniques", in Proceedings of the 1st Annuaol Conference on Astronomical Data Analyses Software and Systems, NOAO, Tucson, AZ.

8. Collaboration with MLS Co-I Richard Cofield of the Jet Propulsion Laboratory, California Institute of Technology, Pasadena CA.

9. Collaboration with Peter Forkman of Chalmers University of Technology, Gothenburg, Sweden

10. Premier-CORSA Final Report, ESA Contract No.: 4200022848/09/NL/C7, November 2013.

11. Langseth, M.G. Jr., S.P. Clark Jr., J.L. Chute Jr., S.J. Keihm, and A.E. Wechsler (1972), Heat Flow Experiment, in *Apollo 15 Preliminary Science Report*, Section 11, NASA SP-229, U.S. Gov't. Printing Office, Washington, D.C., pp. 11-1 - 11-23.

12. Langseth, M.G., S.J. Keihm , and J.L. Chute Jr., (1973), Heat-flow experiment. In *Apollo 17 Preliminary Science Report*, pp. 9-1 to 9-24, NASA pub. SP330, U.S. Gov't. Printing Office, Washington D.C.

13. Keihm, S.J., J.L. Chute Jr., K. Peters, and M.G. Langseth Jr. (1973), Apollo 15 measurement of lunar surface brightness temperatures: Thermal conductivity of the upper 1.5 meters of regolith, Earth and Planet. Sci. Letters, Vol. 19, pp. 337-351.

14. Keihm, S.J. and M.G. Langseth (1973), Surface brightness temperatures at the Apollo 17 heat flow site: Thermal conductivity of the upper 15 cm of regolith, Proc. Lun. Sci. Conf. 4th, pp. 2503-2513.

15. Langseth, M.G., S.J. Keihm, and K. Peters (1976), The revised lunar heat flow values, Proc. Lunar Sci. Conf. 7th, Geochimica et Cosmochimica Acta, Vol. 3, The Moon and Other Bodies, pp. 3143-3171.

16. Birkebak, R.C. (1974), Thermophysical properties of lunar materials from the Apollo missions, in *Advances in Heat Transfer* (T.F. Irvine, Jr., and J.P. Harner, Eds, Vol. 10, pp. 1-37, Academic Press, New York.

17. Horai, K., J.L. Winkler Jr., S.J. Keihm, M.G. Langseth, and J.A. Fountain (1977), Thermal conductivity of two Apollo 17 drill-core samples 70002 and 70006: A preliminary result, Proc. Lunar Sci. Conf. 8th, abstract, pp. 455-456.

18. Robie, R.A., B.S. Hemingway, and W.H. Wilson (1970), Specific heats of lunar surface materials from 90 to 35 degrees Kelvin, Science 167, pp. 749-750.

19. Carrier, W.D. III, S.W. Johnson, L.H. Carrasco, and R. Schmidt (1972), Core sample depth relationships Apollo 14 and 15, Proc Lunar Sci. Conf. 3rd, pp. 3213-3221.

20. Carrier, W.D. III, J.K. Mitchel, and A. Mahmood (1973), The relative density of lunar soil, Proc. Lunar Sci. Conf. 4th, 2403-2411.

21. Clegg, P.E., Pandya, S.J., Foster, S.A., and Bastin, J.A. (1972), Far infrared properties of lunar rock, Proc. Lunar Sci. Conf. 3rd, pp. 3035-3045.

22. Katsube, T.J. and Collett, L.S. (1973), Electrical characteristics of Apollo 16 lunar samples, Proc. Lunar Sci. Conf. 4th, pp. 3101-3110.

23. Bassett, H.L. and R.G. Shackleford (1972), Dielectric properties of Apollo 14 lunar samples at microwave and millimeter wavelengths, Proc. Lunar Sci. Conf. 3rd, pp. 3157-3160.

24. Birkebak, R.C. and C.J. Cremers (1970), Directional spectral and total reflectance of lunar material,Proc. Apollo 11 Lunar Sci. Conf. V. 3, pp. 1993-2000.

25. Gold, T., F. Bilson, and R.I. Baron (1976), Electrical of Apollo 17 rock and soil samples and a summary of the electrical properties of lunar materials at 450 MHz frequency, Proc. Lun. Sci. Conf. 7th, pp. 2993-2603.

26. Bussey, H.E. (1979), Microwave dielectric measurements of lunar soil with a coaxial line resonator method, Proc. Lunar Sci. Conf. 10th, pp. 2175-2182.

27. Keihm, S.J. and M.G. Langseth (1975), Lunar microwave brightness temperature observations reevaluated in the light of Apollo program findings, Icarus, Vol. 24, pp. 211-230.

28. Keihm, S.J. and M.G. Langseth Jr. (1975), Microwave emission spectrum of the moon: Mean global heat flow and average depth of the regolith, Science, Vol. 187, pp. 64-66.

29. Gary, B.L. and S.J. Keihm (1978), Interpretation of ground-based microwave measurements of the moon using a detailed regolith properties model, Proc. Lunar Plan. Sci. Conf IX, pp. 2885-2900.

30. Keihm, S.J. and B.L. Gary (1979), Comparison of theoretical and observed l3.55 cm brightness temperature maps of the full moon, Proc. Lunar Plan. Sci. Conf. X, pp. 2311-2319.

31. Vasavada, A. R., J. L. Bandfield, B. T. Greenhagen, P. O. Hayne, M. A. Siegler, J.-P. Williams, and D. A. Paige (2012), Lunar equatorial surface temperatures and regolith properties from the Diviner Lunar Radiometer Experiment, J. Geophys. Res., 117, E00H18, doi:10.1029/2011JE003987.

32. Keihm, S.J. (1984), Interpretation of the lunar microwave brightness temperature spectrum: Feasibility of orbital heat flow mapping, Icarus, Vol. 60, pp. 568-589.

33. Keihm, S.J. and J.A. Cutts (1981), Vertical structure effects on planetary microwave brightness temperature measurements: Applications to the lunar regolith, Icarus, Vol. 48, pp. 201-229.

34. Keihm, S.J. (1982), Effects of subsurface volume scattering on the lunar microwave brightness temperature spectrum, Icarus, Vol. 52, pp. 570-584.